Journal of Environmental Chemical Engineering 9 (2021) 106202

Contents lists available at ScienceDirect

Journal of Environmental Chemical Engineering

journal homepage: www.elsevier.com/locate/jece

Monitoring the effect of surface functionalization on the CO_2 capture by graphene oxide/methyl diethanolamine nanofluids

Zongming Zhou [a], Ehsan Davoudi [b], Behzad Vaferi [b,*]

[a] Hanergy (Qingdao) Lubrication Technology Co., Ltd
[b] Department of Chemical Engineering, Shiraz Branch, Islamic Azad University, Shiraz, Iran

ARTICLE INFO

Editor: Dr. Zhang Xiwang

Keywords:
CO_2 capture
Graphene oxide/methyldiethanolamine nanofluids
Surface functionalization
Connectionist paradigms

ABSTRACT

Different processes exist to capture carbon dioxide (CO_2) and reduce its undesirable effects on the atmosphere. Stable suspensions of graphene oxide (GO) nanosheets in aqueous methyl diethanolamine (MDEA) solutions have recently attracted great attention as a potential CO_2 absorption medium. Moreover, experimental analyses confirmed that GO surface functionalization positively affects the CO_2 absorption by MDEA-based nanofluids. To the best of our knowledge, there are no mathematical models to investigate the effect of surface functionalization on the CO_2 capture ability of GO-amine nanofluids. Artificial intelligence (AI) techniques are reliable methodologies for understanding behavior of even the most complex systems. Therefore, different AI models are designed to reveal the effect of GO surface functionalization on the CO_2 capture ability of MDEA-based nanofluids. Our AI models use operating temperature, pressure, functionalized group, and GO dosage in the amine solutions to predict CO_2 solubility in GO/MDEA nanofluids. The results confirm that the cascade feedforward (CFF) neural network is the most accurate AI paradigm for estimating CO_2 solubility in aqueous GO/MDEA nanofluids in a wide range of operation conditions (i.e., AARD = 1.78%, MSE = 0.007, RMSE = 0.08, and R^2 = 0.9906). Simulation results justified that the surface functionalization of the GO nanosheets by the NH_2 group provides the most promising results for CO_2 capture by the GO/MDEA nanosuspensions.

1. Introduction

Mass transfer is one of the main branches of classical physics resulting from a concentration gradient in single or multiphase systems [1]. Mass transfer by convection or diffusion mainly occurs in separation processes to capture valuable/undesirable ingredients from a stream [2–4]. Absorption is one of the most popular operation units to separate one or more substances from a gas mixture by a liquid [5]. The performance of absorption units is usually determined by their ability to separate/capture considered substances from a gas stream [6]. Greenhouse gas (carbon dioxide, carbon monoxide, methane, nitrous oxide, hydrofluorocarbons, perfluorocarbons, sulfur hexafluoride, and nitrogen trifluoride) emissions are among the main concerns of researchers for more than a century [7,8]. Carbone dioxide (CO_2) has the most considerable contribution to greenhouse gas emissions [9,10]. Its cumulative emission from 1850 to 2019 was estimated to be 2340 ± 240 gigatons (70% from the combustion of fossil fuels and 30% from other sources) [11]. Chemical absorption [12], adsorption [13], membrane-based technology [14], and the cryogenic process [15] are the most well-known operations for CO_2 capture. Absorption of carbon dioxide molecules using the aqueous amine solutions is likely the most well-known process in this regard [16].

Nano-scale technology has achieved a wide range of applications in improving the thermophysical characteristics of traditional working fluids [17,18], air pollution reduction [19], catalyst [20], nano-catalyst [21], improving the activated sludge properties [22], and heavy metal removal from aqueous solutions [23]. Hence, some modifications, such as adding nano-sized solid particles to the liquids, are proposed to enhance the CO_2 capture ability of the absorption process [24–26]. The homogeneous suspension of nano-sized solid particles (<100 nm) in a base fluid is known as nanofluid [27,28]. Elhambakhsh and Keshavarz dispersed six different magnetic nanoparticles in the aqueous N-Methyl-2-pyrrolidone solution to enhance the CO_2 absorption capacity of base fluid [29]. Several experimental measurements of CO_2 solubility in nanofluids in closed vessels are conducted up to now [30–32]. Rahimi et al. investigated the effect of host fluid and hydrophilicity of multi-walled carbon nanotubes (MWCNT) on the CO_2 absorption capacity of an amine-based nanofluid [33]. The CO_2 absorption in the SiO_2

* Corresponding author.
E-mail address: vaferi@iaushiraz.ac.ir (B. Vaferi).

https://doi.org/10.1016/j.jece.2021.106202
Received 10 June 2021; Received in revised form 2 August 2021; Accepted 10 August 2021
Available online 14 August 2021

and ZnO water-based nanofluids is experimentally measured at different temperatures and pressures [34]. The results showed that the solubility of carbon dioxide in ZnO nanofluids is higher than in the SiO_2 nanofluids for all experimental conditions [34]. The addition of 0.1 wt percent (wt %) of nano-sized Al_2O_3 and SiO_2 to pure water increases its CO_2 absorption capacity by 18% and 21%, respectively. Carbon nanotubes and Fe_3O_4 were more effective at 0.02 wt% nanoparticle concentration, and they could increase it up to 34% and 24%, respectively [35]. Moreover, methyl diethanolamine/carbon nanotubes enhance the absorption capacity of CO_2 by up to 23% [35]. The transient and equilibrium absorption of carbon dioxide in functionalized multi-walled carbon nanotubes and Fe_3O_4 nanoparticles suspensions in the Sulfinol-M are also experimentally studied [36]. The maximum enhancement of 46.7% and 23.2% are observed for the absorption rate and equilibrium solubility, respectively. Graphene oxide/MDEA nanofluid showed high absorption capacities toward CO_2. The absorption capacity of N-methyl diethanolamine aqueous solution is increased by 9.1% and 10.4% during the addition of 0.1 and 0.2 wt% of graphene oxide (GO) [24]. This absorption increases by increasing pressure and decreasing temperature [24]. Alivand et al. enhanced the carbon dioxide capture capacity of aqueous N, N-diethylethanolamine (DEEA) solutions by adding several nano-porous carbonaceous promoters [37]. The CO_2 solubility in aqueous MDEA solutions with and without GO nanosheets is studied [38]. The authors claimed that GO and its functionalized form increase the CO_2 adsorption capacity of the MDEA solution up to 12.5% and 7.5%, respectively [38]. Irani et al. dispersed the amine-functionalized GO nanoparticles in MDEA aqueous solution (i.e., NH_2-GO/MDEA nanofluid) and investigated its H_2S and CO_2 absorption capacity [39]. It is reported that the synthesized nanofluids enhanced H_2S and CO_2 absorption by 17.7% and 16.2%, respectively. The effect of GO and its functionalized form by polyethyleneimine (PEI) on the CO_2 capture capacity of MDEA solution is investigated experimentally [40]. It was observed that the PEI-GO nanoparticles could improve CO_2 absorption by 15%. Both solubility and mass transfer rate of carbon dioxide in monoethanolamine (MEA) were tried to model in terms of some dimensionless numbers [41]. Lai et al. investigated the effect of dispersion of functionalized SiO_2 nanoparticles in the 3–aminopropyltrimethoxysilane to improve its CO2 absorption ability [42]. The capacity of homogeneous suspensions of titanium dioxide (TiO_2) and GO nanoparticles in the MEA in the presence of surfactants to absorb CO_2 are also investigated [43].

1.1. Motivation and novelty of our study

Since carbon dioxide mainly contributes to the greenhouse gas effects, its efficient removal before releasing into the atmosphere is essential for industrial and real-life applications [44]. High selectivity, low regeneration energy, high stability, and low corrosion problem of the aqueous MDEA solutions introduced them as efficient media for CO_2 absorption [24]. Experimental studies approved that dispersing GO nanosheets in the MDEA solutions may enhance their CO_2 absorption capacity [24,45]. Moreover, GO surface modification by different functionalized groups is recently proposed to intensify the CO_2 capture ability of the MDEA-based medium. No mathematical models or experimental evidence are available to investigate the effect of GO functionalization on the CO_2 capture capacity of the MDEA-based nanofluids. Therefore, the current study aims to reveal the dependence of the CO_2 capture capacity of the MDEA-based nanofluids on the functionalization of the GO nanosheets using different AI techniques. This modeling study easily compares the enhancing effect of different functionalized groups on the carbon dioxide capture ability of the MDEA aqueous solution. Moreover, the effects of operating conditions (pressure and temperature) and GO dosage in the MDEA solutions on the CO_2 removal are also investigated from modeling and experimental perspectives.

2. Artificial intelligent methods

Effects of GO functionalization on the CO_2 capture capacity of MDEA-based nanosuspensions are simulated using different AI techniques. The least-squares support vector machines (LSSVM), adaptive neuro-fuzzy inference systems (ANFIS), generalized regression (GR), radial basis function (RBF), CFF, and multilayer perceptron (MLP) neural networks are applied to the intelligent simulation of the considered matter. Some concise information about these intelligent paradigms are given in this section.

2.1. Artificial neural networks (ANN)

The artificial neural networks are initially developed by simple simulation of the working route of the neurological system of humankind [46]. Like biological systems, the neuron is the smallest meaningful part of the ANNs [47]. The artificial neurons use the simple mathematical operation to simulate the working procedure of the biological neurons as follows [48]:

$$net = \sum_{r=1}^{N} w_{mr}\, x_r + b_m \tag{1}$$

$$out_m = f(net) \tag{2}$$

The above equation states that the entry information to a neuron (x_r) multiply by their weights (w_{mr}) and bias (b_m) adds to their summation ($\sum_{r=1}^{N} w_{mr}\, x_r$) to produce net input ($net$). This linear mathematical operation then passes through a transfer or activation function (f) to produce the neuron outlet (out_m). In this study, the tangent sigmoid, logarithms sigmoid, Gaussian, and linear is used as activation functions in different ANN models. Eqs. (3)–(6) express the mathematical formulations of these activation functions, respectively [49].

$$f(net) = \frac{e^{net} - e^{-net}}{e^{net} + e^{-net}} \tag{3}$$

$$f(net) = \frac{1}{1 + e^{-net}} \tag{4}$$

$$f(net) = e^{\frac{-net^2}{2\,\sigma^2}} \tag{5}$$

$$f(net) = net \tag{6}$$

here, σ stands for the spread of the Gaussian activation function.

Therefore, it is possible to construct different artificial networks by systematically connecting neurons in some successive layers. Even though arbitrary numbers of layers may be used for the ANN models, they often have three layers, i.e., input, hidden, and output [3]. The independent and dependent variables constitute the input and output layers, respectively. It is also necessary to place enough neurons between input and output layers, i.e., hidden neurons. Moreover, activation functions for hidden and output layers are required to be determined. In this study, the tangent sigmoid and logarithms sigmoid functions are used in the hidden and output layers of the MLP and CFF neural networks, respectively. Furthermore, the Gaussian and linear functions are used in hidden and output layers of the RBF and GR neural networks, respectively.

2.2. Adaptive neuro-fuzzy inference systems

The ANFIS model can be seen as systematic cooperation between the fuzzy inference and ANN methodologies [50]. This combination aims to preserve the advantages of fuzzy inference and ANN models and cover their limitations [51]. The ANFIS structure is often engineered using five successive layers, i.e., two adaptive (1 and 4) and three fixed (2, 3, and 5) layers [52,53].

2.3. Least-squares support vector machines

The support vector machines (SVM) transforms the raw independent variables into a multidimensional space using the kernel function [54]. Different kernel functions, including linear, polynomial, and Gaussian are widely employed in the SVM-based modeling studies [55]. In this multidimensional space, it is possible to relate dependent to independent variables using a linear formula. If the least-squares technique is used to adjust the SVM model's unknown parameters, it appears as the LSSVM methodology.

2.4. Learning process

The process that tries to adjust the AI-based models' unknown parameters using an appropriate optimization algorithm is known as the training or learning stage. During this stage, the AI-based model is provided with both independent and dependent variables. After that, the optimization technique adjusts the AI model's unknown parameters by minimizing the observed deviation (between independent variables and their predictions). In this study, eleven different training algorithms are applied to adjust the hyper-parameters of the ANN models. Back-propagation and hybrid optimization methods are also employed to train the ANFIS model. The least-squares method is also used during the learning stage of the LSSVM models.

2.5. Experimental stage

This study aims to introduce an intelligent model to investigate the effect of GO surface functionalization on the CO_2 capture ability of GO/MDEA nanofluids. Indeed, this study is a pure simulation work that analyzed reported experimental measurements in the literature employing AI techniques [24,38–40]. Meanwhile, it is better to review the experimental procedure and characterization tests reported in the source articles of the collected experimental database [24,38–40].

2.5.1. Material characterization

X-ray diffraction (XRD), Brunauer–Emmett–Teller (BET), scanning electron microscope (SEM), Fourier-transform infrared spectroscopy (FTIR), thermogravimetric analysis (TGA), x-ray photoelectron spectroscopy (XPS), energy-dispersive x-ray spectroscopy (EDX or EDS), and zeta potential are the characterization tests available in the source articles of the collected database [24,38–40]. Table 1 summarizes the conducted characterization tests in each text. These tests were conducted to characterize the GO nanosheets, functionalized GO nanosheets, and GO/MDEA nanofluids. It should also be mentioned that diethylenetriamine (DETA), amine (NH_2), and polyethyleneimine (PEI) groups are used to surface modification of the GO nanosheets.

Although further information is possible to achieve from the sources articles [24,38–40], it is better to review some key results here. The XRD, BET, and TGA illustrate the average crystalline property, surface characteristics, and thermal stability of the GO nanosheets (and their functionalized form). The SEM reveals the morphology of GO nanosheets and their functionalized forms. The FTIR test is applied to monitor the inherent functional groups of the GO nanosheets and their new attached groups during surface modification. The XPS analyzes the chemical state and atomic ratio of each element in the GO nanosheets and their functionalized forms. The EDX shows the elemental composition of GO nanosheets and their functionalized forms. Zeta potential analysis measures the stability level of the synthesized GO/MDEA nanofluids.

2.5.2. Experimental procedure for CO_2 capture by GO/MDEA nanofluids

Reviewing the source articles shows that the GO nanosheets were synthesized by the modified Hummers method [56]. Then the surface modification was performed to attach DETA, NH_2, or PEI group on the GO nanosheets [24,38–40]. Different tests, including XRD, BET, FTIR, SEM, EDX, TGA, and XPS, were then conducted to characterize both GO nanosheets and their functionalized forms. The absorption medium was prepared by adding the synthesized GO nanosheets (or the functionalized form) to the MDEA solution (40 wt% MDEA in water). The ultrasonic agitation was employed to homogenize the nanosuspension. The zeta potential is applied to check the stability of the GO/MDEA nanosuspension. Finally, the CO_2 solubility in the synthesized absorption medium was experimentally measured in the equilibrium cell [24,38–40]. The effect of functionalized groups of the GO nanosheets, GO dosage in the aqueous amine, pressure, and temperature on the absorption ability of the GO/MDEA were monitored by experimentations [24,38–40].

2.5.3. Literature data

The vapor-liquid equilibrium and published literature state that the solubility of CO_2 in GO/MDEA nanofluids depends on temperature, pressure, the dosage of GO in the MDEA solutions, and surface functionalization of the GO nanosheets [24,38–40]. In this study, 298 experimental datasets for solubility of CO_2 in GO/MDEA nanosuspensions are collected from four different literatures [24,38–40]. The collected experimental database summary, including feature and response variables, their ranges, and the number of available data, is presented in Table 2. The experimental datasets include five different absorption media, i.e., MDEA aqueous solution, GO/MDEA, DETA-GO/MDEA, PEI-GO/MDEA, and NH_2-GO/MDEA nanosuspensions. Moreover, the temperature and pressure ranges are 303.15–333.15 K and 2.05–23.79 bar[1], respectively [24,38–40].

2.5.4. Influence of GO nanosheets on the CO_2 absorption

It is widely accepted that the reaction between MDEA and CO_2 molecules is generally slow, but either increasing pressure or decreasing temperature can enhance it. Several mechanisms are available to explain the reaction between carbon dioxide and MDEA molecules in the aqueous solution [40]. The first mechanism states that MDEA neutralizes the products of the water-CO_2 reactions. The second one states that MDEA associates with water molecules before starting a reaction with carbon dioxide molecules. The third one that is based on the zwitterion mechanism involves forming a zwitterion in the presence of GO nanosheets. It is then followed by formation of the carbamate by the base-catalyzed deprotonation of the zwitterion.

Indeed, the hydrodynamic, bubbles breaking, and grazing effects are the scientific evidence that confirm the mass transfer coefficient increases during homogeneous dispersion of GO nanosheets in the MDEA solution [40]. The hydrodynamic effect states that the nanosheets' collision with the gas-liquid interface decreases both interface thickness and mass transfer resistance. This phenomenon finally increases the diffusion coefficient between gas and liquid phases and improves the CO_2 capture ability of the absorption medium. The bubbles breaking effects said that the gas bubble sizes decrease during their collision with the GO nanosheets. The collisions also result in increasing the turbulency in the absorption medium. Combining these phenomena increases the mass transfer coefficient and CO_2 absorption ability of the GO/MDEA nanosuspensions. The grazing effect mechanism explains that the GO nanosheets move to the gas-liquid interface, adsorb gas bubbles, transfer them into the bulk liquid, and finally desorbs the adsorbed gas into the liquid phase. Obviously, the nanoparticles have a central role in transferring the CO_2 molecules from gas to the MDEA phase and improving the separation efficiency.

2.6. Pre-processing on the collected databank

Our previous experiences confirmed that it is possible to simplify the training stage, increase its convergence rate, and reduce the possibility

[1] Absolute pressure.

Table 1
Available characterization tests in the source articles of the collected database.

Absorption media	XRD	BET	SEM	FTIR	TGA	XPS	EDX	Zeta potential	Ref.
MDEA + GO	✓	✓	✓	✓	×	×	✓	✓	[24]
MDEA + DETA-GO	✓	✓	✓	✓	✓	×	✓	✓	[38]
MDEA + NH_2-GO	✓	✓	✓	✓	✓	✓	✓	✓	[39]
MDEA + PEI-GO	✓	✓	✓	✓	✓	✓	✓	✓	[40]

Table 2
Complete information of experimental database [24,38–40].

Absorption liquid	Features				Response	No. of data
	Functionalized group	GO dosage in MDEA (wt%)	Temperature (K)	Pressure (bar)	CO_2 solubility (mol/kg)	
40 wt% aqueous MDEA	–	0	303.15–333.15	2.05–22.12	1.75–4.28	63
40 wt% aqueous MDEA+ graphene oxide	DETA	0.1	303.15–323.15	2.17–23.01	1.85–4.70	27
40 wt% aqueous MDEA+ graphene oxide	NH_2	0.1	303.15–333.15	2.23–23.79	2.10–4.54	36
40 wt% aqueous MDEA+ graphene oxide	–	0.1–0.2	303.15–333.15	2.13–23.12	1.78–4.41	99
40 wt% aqueous MDEA+ graphene oxide	PEI	0.1–0.2	303.15–333.15	2.13–21.38	1.99–4.27	72

of saturation of AI-based model parameters by scaling feature and response variables [57–60]. Thus, Eq. (7) is applied to scale all variables to the 0.01–0.99 domain.

$$\overline{V} = 0.01 + 0.98 \times \frac{V - V^{\min}}{V^{\max} - V^{\min}} \tag{7}$$

here, V shows the original value of a variable, $\overline{V}$ is its normalization, $V^{\min}$ and $V^{\max}$ are their minimum and maximum values.

3. Results and discussion

This section aims to find (1) an appropriate transformation for solubility of CO_2 in GO/MDEA nanosuspensions, (2) the best structure of the considered AI-based approaches, (3) an appropriate training algorithm for adjustment on AI model's parameters, (4) the effect of surface functionalization of on the CO_2 absorption capacity of the GO/MDEA solutions.

3.1. Selection of the best transformation for the dependent variable

From the modeling point of view, it is sometimes better to work with a transformed version of the response variable than its original form [61]. Estimation of vapor pressure by Antoine's equation is likely the most well-known example of this type of transformation (it provides the natural logarithm of vapor pressure rather than its simple form). Pearson's technique is a reliable tool to find the most appropriate transformation for a given modeling study [61]. This technique illustrates the direction and strength of the response's dependence on a particular feature by a factor range from −1 to +1. The maximum and minimum factors (i.e., +1 and −1) show the strongest direct and indirect relationship between the response and feature variable, respectively. Similarly, the zero factor associates with no relation between the concerned variables. Therefore, higher absolute factors are preferred in the modeling study. For modeling multi-input and single-output systems, it is better to consider the average of absolute Pearson's coefficients (AAPC) obtained for all possible pairs of response/feature variables.

Fig. 1 presents AAPC values for different transformations of the CO_2

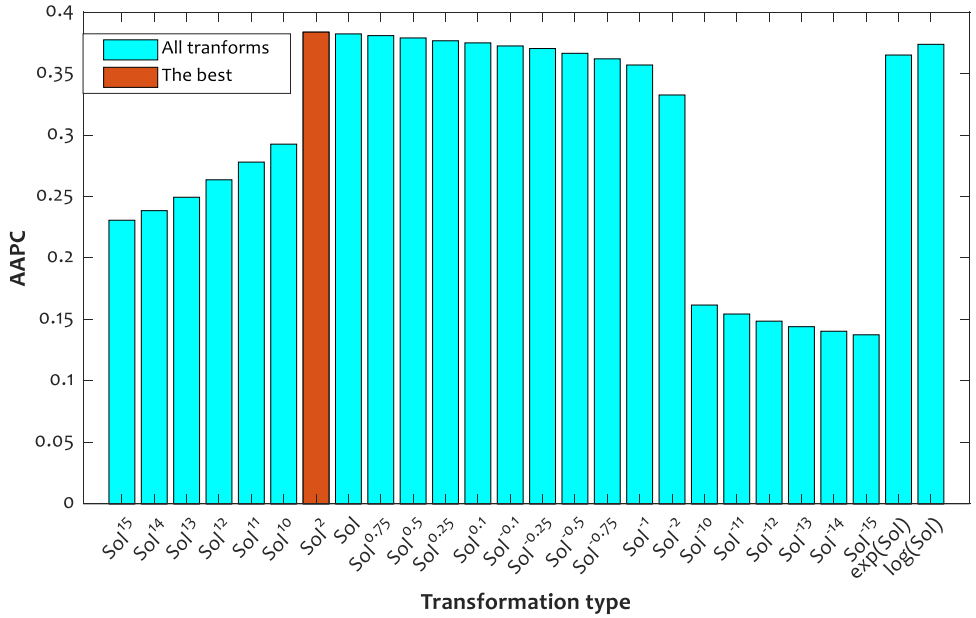

Fig. 1. Finding the most appropriate transformation for the CO_2 solubility (Sol).

solubility (Sol) in the GO/MDEA nanosuspensions. This figure confirmed that the transformation affects the strength of dependency of CO_2 solubility to the considered features. Moreover, the seventh transformation (i.e., power of two) has the maximum AAPC value; hence it is the most appropriate transformation for modeling the concerned matter.

Indeed, all AI-based techniques will be developed to estimate the $(CO_2 \text{ solubility})^2$. Finally, this transformation needs to be reverted to achieve the predicted value of CO_2 solubility in the GO/MDEA nanosuspensions.

Table 3 presents the relevancy factor between the CO_2 solubility and the considered features. It can be seen that three out of the four features have a direct influence on the response variable, while the temperature has an indirect effect on the CO_2 solubility. Moreover, pressure and temperature have the strongest direct and indirect influence on the nanosuspensions' CO_2 capture capacity, respectively.

3.2. Finding the most accurate intelligent model

Eighty percent of experimental data are used to adjust unknown parameters of the AI models during the learning stage. The remaining twenty percent are utilized for checking the performances of the trained models. This study designs 1880 different AI models (i.e., 350 MLP, 350 CFF, 350 RBF, 50 GR, 480 ANFIS, and 300 LSSVM models), compares their results, and finally introduces the best one. Table 4 reports the most accurate results obtained by the particular intelligent model. The efficiency of models is measured in terms of absolute average relative deviation (AARD%), mean squared errors (MSE), root mean squared errors (RMSE), and regression coefficient (R^2) over the training, testing, and whole of the database.

Table 4 shows that a single hidden layer CFF neural network with seven neurons (the highlighted section) is the most efficient AI model for estimating the CO_2 solubility in GO/MDEA nanosuspensions. This model predicted 297 experimental datasets with AARD = 1.78%, MSE = 0.007, RMSE = 0.08, and R^2 = 0.9906. This model's excellent performance can also be justified by its prediction for testing datasets, i.e., AARD = 2.2%, MSE = 0.01, RMSE = 0.1, and R^2 = 0.9882.

The effect of training algorithms on the best AI model's predictions also needs to be investigated. For doing so, the CFF neural networks are trained by ten new training algorithms, and the obtained results are compared in terms of accuracy and training time. Table 5 presents the most accurate results obtained by different training algorithms and their computational training time. The AARDs of training, testing, and overall dataset and computational time per iteration are reported for the considered algorithms. It is worth noting that these analyses are performed using a personal computer with the specification of Intel Core i7–4500 U CPU @ 1.80–2.40 gigahertz, RAM 4 gigabytes. It can be seen that Levenberg–Marquardt is the best algorithm for adjusting unknown parameters of the CFF neural networks (the highlighted row). On the other hand, the gradient descent with momentum needs the minimum computation effort and shows the worst results for simulating the considered problem. The accuracy of the CFF model trained by Levenberg–Marquardt is so good that its relatively high computational time seems unimportant.

Therefore, the cascade feedforward neural network with seven hidden neurons trained by the Levenberg–Marquardt algorithm is selected as the most reliable AI model for estimating the CO_2 solubility in GO/MDEA solutions. This CFF model with optimum topology will be used as the intelligent core in all the subsequent analyses.

As mentioned earlier, the training algorithm adjusts the unknown parameters of the AI model during an iterative procedure. It continuously monitors the deviation between actual and predicted CO_2 solubility, backpropagates this deviation inside the AI model, and updates its unknown parameters' values. Performance of the Levenberg–Marquardt for adjusting the CFF parameters in terms of MSE versus iteration is depicted in Fig. 2. The observed MSE between experimental and predicted values of CO_2 solubility decreases gradually by increasing numbers of iterations, and it finally converges to the predefined desired MSE value. The best MSE value of 0.00075 is obtained after 1000 iterations.

Table 3
Degree of relevancy between the dependent and independent variables.

Independent variables	Relevancy factor
Type of surface modification	0.131
Concentration of GO nanosheets in MDEA solutions (wt%)	0.152
Temperature (K)	−0.551
Pressure (bar)	0.701

3.3. Accuracy assessment of the CFF model

Graphical presentation of CFF neural network model performance for estimating CO_2 solubility during training (red hexagram symbols) and testing (black diamond symbols) stages is presented in Fig. 3. Three straight lines associated with the −7%, exact prediction, and +7% deviations are also added to this figure. This figure said that almost all datasets are predicted with the AARD ranges from −7 to +7%. Moreover, an accumulation of the training and testing symbols around the diagonal line is an indicator for approval of the intelligent model's excellent performance. The regression coefficient close to one for both training and testing subdivisions (i.e., 0.9913 and 0.9882) is another factor that justifies the CFF neural network's excellent prediction.

The residual error is another statistical index for measuring the difference between actual and prediction values of a given response variable. It can be simply obtained by subtracting the actual values of the CO_2 solubility in the GO/MDEA nanofluids from their predictions by the proposed CFF model. The histogram of the residual error of the CFF model is depicted in Fig. 4. This figure explains that the residual error ranges from −0.3 to +0.3. Moreover, the average value and standard deviation of these residual errors are 0.0026 and 0.083, respectively. These values produce a relatively small uncertainty for predicting CO_2 solubility that ranges from 1.75 to 4.70 mol/kg.

Like all other data-driven models, the cascade feedforward neural network's reliability also depends on the reliability of the experimental database. Therefore, it is necessary to check the validity of the available experimental data before applying the designed CFF model in real situations. The leverage method is a well-known tool to discriminate between valid and outlier data [44]. This method is applied to our experimental data, and its results are presented in Fig. 5. The leverage method approved that only 5 out of 297 are the outlier (red circle symbols), and the rest is valid. Since the numbers of outliers are too small, their negative effect on the designed CFF neural network model's generalization ability could be neglected. Therefore, this AI-based model is designed by a valid database and can be readily used in real applications.

3.4. Analyzing the effect of influencing factors

Fig. 6 explains the dependency of the CO_2 capture capacity of MDEA-based nanofluids on the operating pressure for two different GO dosages from both experimental and modeling perspectives. An excellent agreement between actual measurements and CFF predictions can be concluded from this figure. The AARD of 0.89% and 0.61% is observed to estimate the CO_2 capture capacity of MDEA containing 0.1 and 0.2 wt % of GO nanosheets, respectively.

This figure shows that the mass concentration of the GO nanosheets has little influence on the CO_2 capture capacity of the MDEA-based nanosuspensions. This observation is in complete agreement with the experimental results reported by Irani et al. [24]. On the other hand, the GO/MDEA nanofluids' tendency to absorb CO_2 gradually increases by increasing the operating pressure. Increasing the operating pressure from 2 to 22 bar enhances the nanofluids' absorption capacity by 58%.

Table 4
The most accurate results obtained by different intelligent approaches.

AI Model	Specification of developed models	Specification of the best model	Database	AARD %	MSE	RMSE	R^2
MLP	350 models (1–7 hidden neurons, trained by Levenberg–Marquardt)	One hidden layer with 6 neurons	Train	2.21	0.010	0.10	0.9872
			Test	2.40	0.013	0.11	0.9810
			Total	2.25	0.010	0.10	0.9861
CFF	350 models (1–7 hidden neurons, trained by Levenberg–Marquardt)	One hidden layer with 7 neurons	Train	1.68	0.006	0.08	0.9913
			Test	2.20	0.010	0.10	0.9882
			Total	1.78	0.007	0.08	0.9906
RBF	350 models (1–7 hidden neurons, $1 \times 10^{-6} <$ spread < 10)	One hidden layer with 7 neurons and spread = 2.449	Train	4.16	0.043	0.21	0.9425
			Test	4.19	0.046	0.22	0.9285
			Total	4.17	0.043	0.21	0.9397
GR	50 models (238 hidden neurons, $1 \times 10^{-6} <$ spread < 10)	One hidden layer with 238 neurons and spread = 0.1	Train	3.27	0.024	0.15	0.9697
			Test	3.79	0.031	0.18	0.9531
			Total	3.37	0.025	0.16	0.9666
ANFIS	480 models (2–7 clusters, trained by different algorithms)	Seven clusters, hybrid algorithm	Train	2.51	0.014	0.12	0.9817
			Test	2.77	0.016	0.13	0.9743
			Total	2.56	0.014	0.12	0.9804
LSSVM	300 models (different kernel functions)	Polynomial kernel function	Train	1.77	0.007	0.09	0.9905
			Test	2.23	0.011	0.11	0.9821
			Total	1.86	0.008	0.09	0.9891

Table 5
Influence of training algorithm on the performance of the CFF neural network.

Training algorithm	AARD%			Training time (ms/ iteration)
	Training	Testing	Overall	
Levenberg–Marquardt	1.68	2.20	1.78	3.565
BFGS quasi-Newton	2.51	2.89	2.59	7.770
Scaled conjugate gradient	2.93	2.83	2.91	1.334
Conjugate gradient backpropagation with Powell-Beale restarts	2.99	3.03	3.00	2.262
Conjugate gradient backpropagation with Polak-Ribiere updates	3.39	3.50	3.41	3.070
One-step secant	3.33	3.79	3.42	1.107
Bayesian regulation	3.38	3.70	3.44	2.841
Gradient descent with momentum and adaptive learning rate	3.30	4.89	3.62	1.110
Gradient descent with adaptive learning rate	4.32	5.03	4.46	1.237
Gradient descent backpropagation	10.74	12.19	11.03	1.148
Gradient descent with momentum	12.62	11.02	12.30	1.140

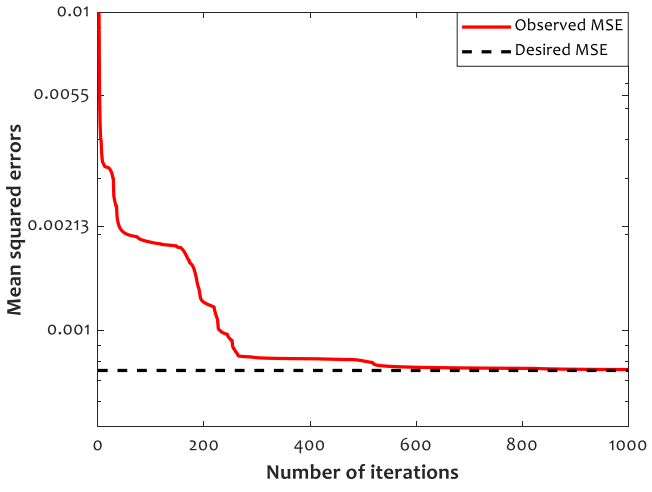

Fig. 2. Profile of MSE versus iteration during the learning process of the CFF model by the Levenberg–Marquardt algorithm.

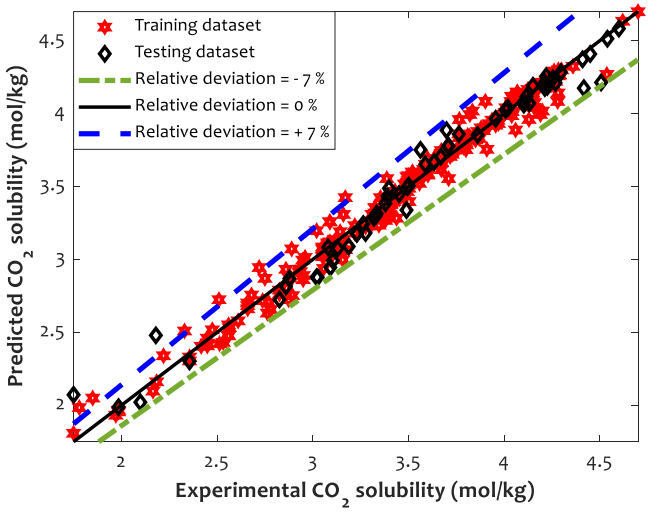

Fig. 3. Cross-plot of prediction versus experimental data of the CO_2 solubility.

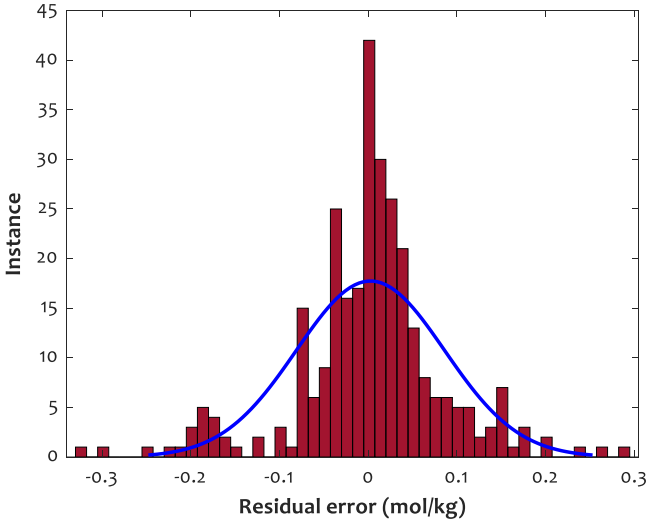

Fig. 4. Histogram of residual error between actual and predicted CO_2 solubility.

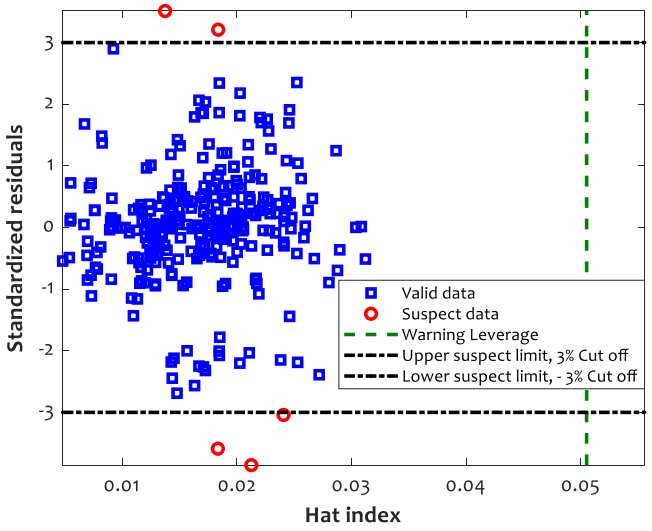

Fig. 5. William's plot for detecting valid and outlier information.

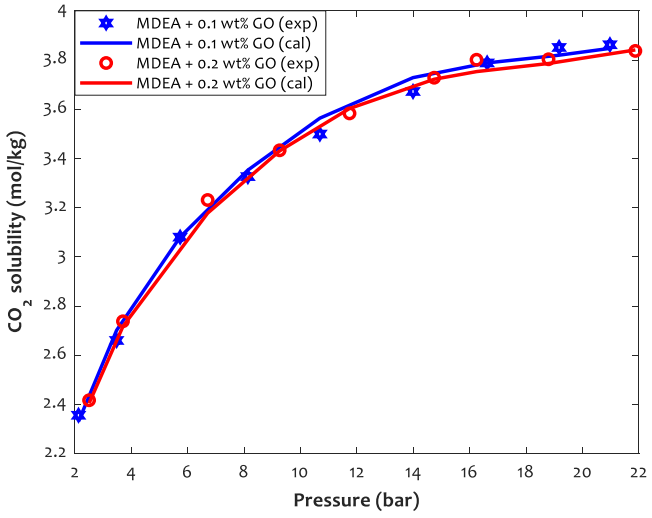

Fig. 6. Investigation of the effect of GO dosage on the CO_2 capture (323 K).

This observation may be related to the increasing gas solubility in the liquid by increasing pressure. Moreover, the driving force for CO_2 transfer from the gas to the liquid phase increases by increasing the pressure [44].

The influence of operating pressure and mass concentration of the PEI-GO nanosheets on the CO_2 capture ability of the MDEA-based nanosuspensions is presented in Fig. 7. The deviation between actual and predicted CO_2 solubilities has the AARD of 0.80% and 1.06%, respectively. It can be seen that the GO and PEI-GO dosages have a relatively similar effect on the CO_2 absorption ability of the MDEA-based nanofluids. Aghehrochaboki et al. observed a completely similar trend in their experimental investigation [40]. The aggregation of GO-PEI nanoparticles when 0.2 wt% is dispersed in the aqueous MDEA solution was introduced as the main reason for this observation [40]. A comparison with the previous graph justified that the functionalization of the GO by the PEI has better performance than the simple GO nanosheets.

The variation of CO_2 solubility in different solutions as a function of pressure is illustrated in Fig. 8. This figure presents both experimental measurements and their associated predictions by the proposed CFF neural network. The AARD of 1.76%, 1.15%, 0.87%, and 0.67% are observed to estimate the CO_2 absorption ability of MDEA, GO/MDEA,

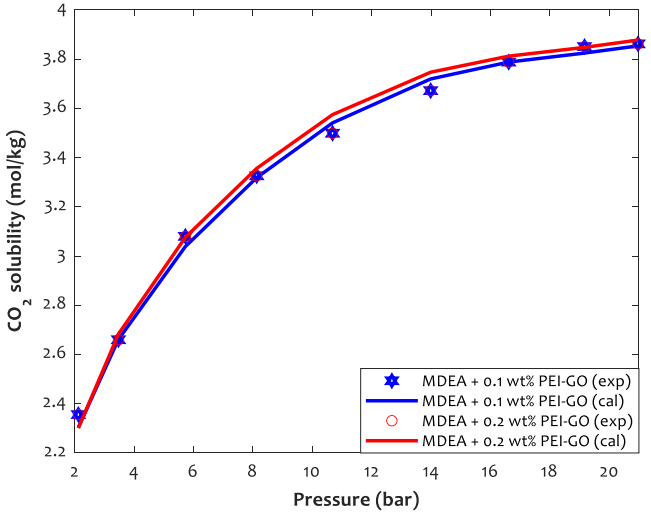

Fig. 7. Investigation of the effect of PEI-GO dosage on the CO_2 capture (323 K).

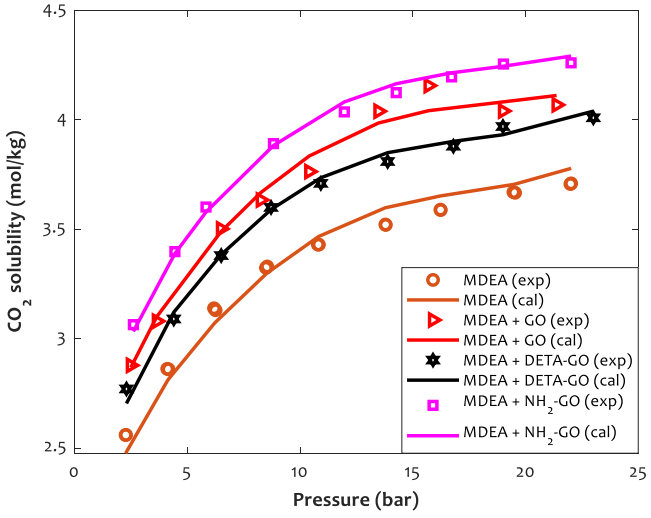

Fig. 8. Influence of GO functionalization on the CO_2 solubility (313 K, 0.1 wt%).

DETA-GO/MDEA, and NH2-GO/MDEA nanosuspensions, respectively.

It can be concluded that all MDEA-based nanofluids have better CO_2 absorption capacity than the simple MDEA solution. The previously conducted experimental studies have reported the same results [24, 38–40]. On the other hand, the GO's surface functionalization by the NH_2 has the most promising effect on improving the MDEA ability for CO_2 absorption. Moreover, the GO/MDEA has a better CO_2 absorption capacity than the DETA-GO/MDEA nanofluids. The considered solution shows the following order for the CO_2 absorption.

$$\text{MDEA-NH}_2\text{/GO} > \text{MDEA-GO} > \text{MDEA-DETA/GO} > \text{MDEA} \quad (8)$$

It is worth noting that no experimental or modeling studies are conducted to compare the effect of GO functionalized groups on the CO_2 capture ability of GO/MDEA nanofluids.

3.5. *Three-dimensional analyses*

In this section, the designed CFF neural network with the optimum structure is employed for simulating the coupling effect of different features on the CO_2 capture capacity of the MDEA-based nanosuspensions.

The coupling effect of pressure and mass concentration of DETA-GO nanosheets on the CO_2 solubility in the MDEA-based nanosuspensions is presented in Fig. 9. This figure states that the CO_2 capture ability of the MDEA-based nanofluids continuously increases by increasing the pressure and mass concentration of DETA-GO nanosheets. Indeed, the maximum CO_2 can be captured in the maximum allowable operating pressure and the highest mass dosage of DETA functionalized GO nanosheets.

The simulation results for the effect of pressure on the CO2 solubility in the nanofluid (MDEA- DETA/GO) agree with the physical evidence. Unfortunately, there are no experimental or modeling findings to validate the simulation observation for the effect of DETA-GO dosage on the CO_2 capture ability of the considered nanofluids.

The simultaneous effect of temperature and pressure on the CO_2 solubility in the GO/MDEA nanosuspensions is illustrated in Fig. 10. It can be seen that the CO_2 capture capacity of the GO/MDEA nanofluids increases by increasing pressure and decreasing temperature. The maximum CO_2 solubility of 4.7 mol/kg could be achieved at the highest allowable pressure and the lowest temperature. Contrary, the lowest pressure and the highest temperature is the condition that minimizes the CO_2 capture capacity of the GO/MDEA nanosuspensions.

The observed simulation results in this section are in agreement with the scientific fact that states gas solubility (here CO_2) in the liquid (here GO/MDEA nanofluid) improves by either increasing the pressure or decreasing the temperature.

Three-dimensional presentation of the CO_2 solubility in DEAT-GO/MDEA nanofluids as a function of temperature and nanoparticle mass dosage is depicted in Fig. 11. The simulation results confirmed that increasing temperature and decreasing mass dosage of nanoparticles negatively affect the nanofluids' CO_2 capture ability. Indeed, the DEAT-GO/MDEA nanofluid shows its worst CO_2 absorption at the maximum temperature and the minimum nanoparticle content.

4. Conclusion

Different artificial intelligent models, including MLP, CFF, RBF, GR neural networks, ANFIS, and LSSVM are developed to estimate the effect of GO surface functionalization on the CO_2 capture ability of MDEA-based nanofluids. Pearson's technique approved that it is better to simulate the $(CO_2 \text{ solubility})^2$ rather than its original value. Therefore, the CO_2 solubility in the nanofluids to the power of two is estimated as a function of temperature, pressure, functionalization group, and GO dosage in the MDEA solution. Results revealed that the CFF neural network is the most accurate smart tool for the considered purpose. The trade-off between the computational time and accuracy approved that the Levenberg–Marquardt is the most efficient algorithm for training the CFF neural network. The proposed model estimated 297 experimental data with the AARD = 1.78%, MSE = 0.007, RMSE = 0.08, and R^2 = 0.9906. This smart model confirmed that the CO_2 capture ability of the MDEA-based nanofluids increases by increasing pressure, decreasing temperature, and increasing the mass concentration of GO nanosheets in the MDEA solution. Moreover, the surface functionalization of GO nanosheets by the NH_2 group increases the CO_2 absorption ability of the MDEA solutions higher than the simple GO, PEI-GO, and DETA-GO nanosheets.

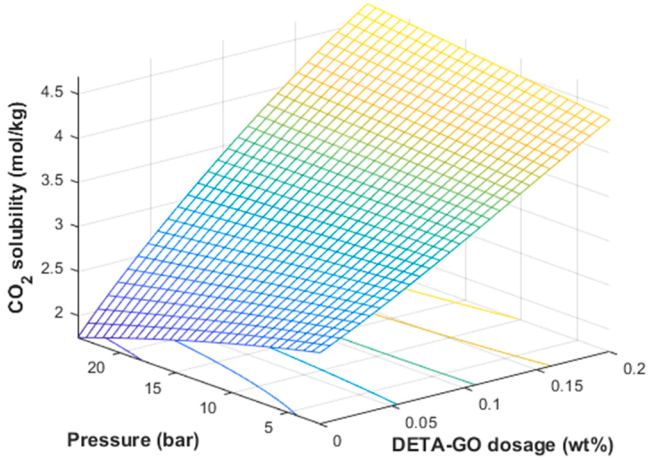

Fig. 9. Variation of CO_2 solubility by variation of pressure and DETA-GO dosage (303 K).

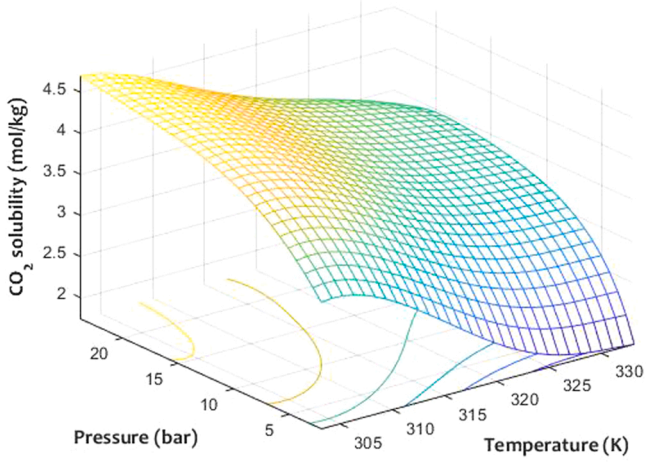

Fig. 10. Three-dimensional variation of CO_2 capture as a function of pressure and temperature (0.1 wt%).

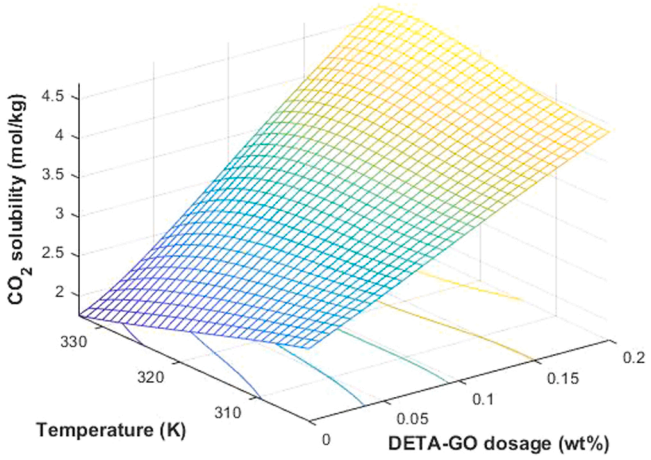

Fig. 11. Variation of CO_2 removal versus temperature and DETA-GO dosage (23 bar).

CRediT authorship contribution statement

Zongming Zhou: Conception/Design, Formal analysis, Writing – review & editing, Resources, Final approval. **Ehsan Davoudi:** Writing – original draft, Data acquisition, Conception/Design, Formal analysis, Resources, Final approval. **Behzad Vaferi:** Writing – original draft, Data acquisition, Conception/Design, Formal analysis, Writing – review & editing, Resources, Final approval supervision.

Declaration of Competing Interest

The authors declare that they have no known competing financial interests or personal relationships that could have appeared to influence

the work reported in this paper.

References

[1] R.E. Treybal, Mass Transfer Operations, MCGraw-Hill, New York, 1980.
[2] H. Pashaei, A. Ghaemi, CO_2 absorption into aqueous diethanolamine solution with nano heavy metal oxide particles using stirrer bubble column: hydrodynamics and mass transfer, J. Environ. Chem. Eng. 8 (2020), 104110.
[3] B. Vaferi, M. Bahmani, P. Keshavarz, D. Mowla, Experimental and theoretical analysis of the UV/H2O2 advanced oxidation processes treating aromatic hydrocarbons and MTBE from contaminated synthetic wastewaters, J. Environ. Chem. Eng. 2 (2014) 1252–1260.
[4] M.F. Ghazvini, M. Vahedi, S.N. Nobar, F. Sabouri, Investigation of the MOF adsorbents and the gas adsorptive separation mechanisms, J. Environ. Chem. Eng. (2020), 104790.
[5] M.M. Raznahan, S. Riahi, S.H. Mousavi, A simple, robust and efficient structural model to predict CO_2 absorption for different amine solutions: concern to design new amine compounds, J. Environ. Chem. Eng. 8 (2020), 104572.
[6] M. Afkhamipour, M. Mofarahi, A. Rezaei, R. Mahmoodi, C.-H. Lee, Experimental and theoretical investigation of equilibrium absorption performance of CO_2 using a mixed 1-dimethylamino-2-propanol (1DMA2P) and monoethanolamine (MEA) solution, Fuel 256 (2019), 115877.
[7] M.R. Rahimpour, S. Mazinani, B. Vaferi, M.S. Baktash, Comparison of two different flow types on CO removal along a two-stage hydrogen permselective membrane reactor for methanol synthesis, Appl. Energy 88 (2011) 41–51.
[8] N. Shurpali, A.K. Agarwal, V.K. Srivastava, Greenhouse Gas Emissions: Challenges, Technologies and Solutions, Springer, 2018.
[9] D.A. Lashof, D.R. Ahuja, Relative contributions of greenhouse gas emissions to global warming, Nature 344 (1990) 529–531.
[10] K.-S. Kang, The method of capturing CO_2 greenhouse gas in cellulose matrix, J. Environ. Chem. Eng. 1 (2013) 92–95.
[11] P. Friedlingstein, M. Jones, M. O'sullivan, R. Andrew, J. Hauck, G. Peters, W. Peters, J. Pongratz, S. Sitch, C. Le Quéré, Global carbon budget 2019, Earth Syst. Sci. Data 11 (2019) 1783–1838.
[12] W.H. Tay, K.K. Lau, A.M. Shariff, High frequency ultrasonic-assisted chemical absorption of CO_2 using monoethanolamine (MEA), Sep. Purif. Technol. 183 (2017) 136–144.
[13] M. Karimi, L. Zafanelli, J.P.P. Almeida, G.R. Ströher, A.E. Rodrigues, J.A.C. Silva, Novel insights into activated carbon derived from municipal solid waste for CO_2 uptake: synthesis, adsorption isotherms and scale-up, J. Environ. Chem. Eng. 8 (2020), 104069.
[14] F. Suhail, M. Batool, A.T. Shah, S. Tabassum, A.L. Khan, M.A. Gilani, Highly CO_2 selective mixed matrix membranes of polysulfone based on hetaryl modified SBA-16 particles, Sep. Purif. Technol. 258 (2021), 117999.
[15] R.P. Lively, W.J. Koros, J.R. Johnson, Enhanced cryogenic CO_2 capture using dynamically operated low-cost fiber beds, Chem. Eng. Sci. 71 (2012) 97–103.
[16] B. Aghel, S. Sahraie, E. Heidaryan, Comparison of aqueous and non-aqueous alkanolamines solutions for carbon dioxide desorption in a microreactor, Energy 201 (2020), 117618.
[17] A.B. Çolak, O. Yıldız, M. Bayrak, B.S. Tezekici, Experimental study for predicting the specific heat of water based Cu-Al2O3 hybrid nanofluid using artificial neural network and proposing new correlation, Int. J. Energy Res. 44 (2020) 7198–7215.
[18] A.B. Çolak, Experimental study for thermal conductivity of water-based zirconium oxide nanofluid: developing optimal artificial neural network and proposing new correlation, Int. J. Energy Res. 45 (2021) 2912–2930.
[19] H. Wang, T. Song, Z. Li, J. Qiu, Y. Zhao, H. Zhang, J. Wang, Exceptional high and reversible ammonia uptake by two dimension few-layer BiI3 nanosheets, ACS Appl. Mater. Interfaces 13 (2021) 25918–25925.
[20] W.-Y. Huang, G.-Q. Wang, W.-H. Li, T.-T. Li, G.-J. Ji, S.-C. Ren, M. Jiang, L. Yan, H.-T. Tang, Y.-M. Pan, Porous ligand creates new reaction route: bifunctional single-atom palladium catalyst for selective distannylation of terminal alkynes, Chem 6 (2020) 2300–2313.
[21] Y. Duan, Y. Liu, Z. Chen, D. Liu, E. Yu, X. Zhang, H. Fu, J. Fu, J. Zhang, H. Du, Amorphous molybdenum sulfide nanocatalysts simultaneously realizing efficient upgrading of residue and synergistic synthesis of 2D MoS 2 nanosheets/carbon hierarchical structures, Green Chem. 22 (2020) 44–53.
[22] M. Zhang, L. Zhang, S. Tian, X. Zhang, J. Guo, X. Guan, P. Xu, Effects of graphite particles/Fe3+ on the properties of anoxic activated sludge, Chemosphere 253 (2020), 126638.
[23] R. Chen, Y. Cheng, P. Wang, Q. Wang, S. Wan, S. Huang, R. Su, Y. Song, Y. Wang, Enhanced removal of Co (II) and Ni (II) from high-salinity aqueous solution using reductive self-assembly of three-dimensional magnetic fungal hyphal/graphene oxide nanofibers, Sci. Total Environ. 756 (2021), 143871.
[24] V. Irani, A. Maleki, A. Tavasoli, CO_2 absorption enhancement in graphene-oxide/MDEA nanofluid, J. Environ. Chem. Eng. 7 (2019), 102782.
[25] M.H.K. Darvanjooghi, M.N. Esfahany, S.H. Esmaeili-Faraj, Investigation of the effects of nanoparticle size on CO_2 absorption by silica-water nanofluid, Sep. Purif. Technol. 195 (2018) 208–215.
[26] S.H. Esmaeili-Faraj, M. Nasr Esfahany, Absorption of hydrogen sulfide and carbon dioxide in water based nanofluids, Ind. Eng. Chem. Res. 55 (2016) 4682–4690.
[27] E. Gholami, B. Vaferi, M.A. Ariana, Prediction of viscosity of several alumina-based nanofluids using various artificial intelligence paradigms – comparison with experimental data and empirical correlations, Powder Technol. 323 (2018) 495–506.
[28] M. Hassanpour, B. Vaferi, M.E. Masoumi, Estimation of pool boiling heat transfer coefficient of alumina water-based nanofluids by various artificial intelligence (AI) approaches, Appl. Therm. Eng. 128 (2018) 1208–1222.
[29] A. Elhambakhsh, P. Keshavarz, Effects of different amin-based core-shell magnetic NPs on CO_2 capture using NMP solution at high pressures, J. Nat. Gas Sci. Eng. 84 (2020), 103645.
[30] Z. Zhang, J. Cai, F. Chen, H. Li, W. Zhang, W. Qi, Progress in enhancement of CO_2 absorption by nanofluids: a mini review of mechanisms and current status, Renew. Energy 118 (2018) 527–535.
[31] P. Amani, M. Amani, G. Ahmadi, O. Mahian, S. Wongwises, A critical review on the use of nanoparticles in liquid–liquid extraction, Chem. Eng. Sci. 183 (2018) 148–176.
[32] M.N.A.W.M. Yazid, N.A.C. Sidik, W.J. Yahya, Heat and mass transfer characteristics of carbon nanotube nanofluids: a review, Renew. Sustain. Energy Rev. 80 (2017) 914–941.
[33] K. Rahimi, S. Riahi, M. Abbasi, Effect of host fluid and hydrophilicity of multi-walled carbon nanotubes on stability and CO_2 absorption of amine-based and water-based nanofluids, J. Environ. Chem. Eng. 8 (2020), 103580.
[34] A. Haghtalab, M. Mohammadi, Z. Fakhroueian, Absorption and solubility measurement of CO_2 in water-based ZnO and SiO2 nanofluids, Fluid Phase Equilib. 392 (2015) 33–42.
[35] B. Rahmatmand, P. Keshavarz, S. Ayatollahi, Study of absorption enhancement of CO_2 by SiO2, Al2O3, CNT, and Fe3O4 nanoparticles in water and amine solutions, J. Chem. Eng. Data 61 (2016) 1378–1387.
[36] M. Nabipour, P. Keshavarz, S. Raeissi, Experimental investigation on CO_2 absorption in Sulfinol-M based Fe3O4 and MWCNT nanofluids, Int. J. Refrig. 73 (2017) 1–10.
[37] H.K. Karlsson, H. Makhool, M. Karlsson, H. Svensson, Chemical absorption of carbon dioxide in non-aqueous systems using the amine 2-amino-2-methyl-1-propanol in dimethyl sulfoxide and N-methyl-2-pyrrolidone, Sep. Purif. Technol. 256 (2021), 117789.
[38] A. Maleki, V. Irani, A. Tavasoli, M. Vahidi, Enhancement of CO_2 solubility in a mixture of 40 wt% aqueous N-Methyldiethanolamine solution and diethylenetriamine functionalized graphene oxide, J. Nat. Gas Sci. Eng. 55 (2018) 219–234.
[39] V. Irani, A. Tavasoli, M. Vahidi, Preparation of amine functionalized reduced graphene oxide/methyl diethanolamine nanofluid and its application for improving the CO_2 and H2S absorption, J. Colloid Interface Sci. 527 (2018) 57–67.
[40] R. Aghehrochaboki, Y. Aghdoud Chaboki, S.A. Maleknia, V. Irani, Polyethyleneimine functionalized graphene oxide/methyldiethanolamine nanofluid: preparation, characterization, and investigation of CO_2 absorption, J. Environ. Chem. Eng. 7 (2019), 103285.
[41] A. Mohammadpour, M. Mirzaei, A. Azimi, Dimensionless numbers for solubility and mass transfer rate of CO_2 absorption in MEA in presence of additives, Chem. Eng. Res. Des. 151 (2019) 207–213.
[42] N. Lai, Q. Zhu, D. Qiao, K. Chen, L. Tang, D. Wang, W. He, Y. Chen, T. Yu, CO_2 capture with absorbents of tertiary amine functionalized nano–SiO2, Front. Chem. 8 (2020) 146.
[43] A. Mohammadpour, M. Mirzaei, A. Azimi, S.M. Tabatabaei, Ghomsheh, Solubility and absorption rate of CO_2 in MEA in the presence of graphene oxide nanoparticle and sodium dodecyl sulfate, Int. J. Ind. Chem. 10 (2019) 205–212.
[44] B. Daryayehsalameh, M. Nabavi, B. Vaferi, Modeling of CO_2 capture ability of [Bmim][BF4] ionic liquid using connectionist smart paradigms, Environ. Technol. Innov. 22 (2021), 101484.
[45] M.H. Ghasemi, V. Irani, A. Tavasoli, Amino functionalized ZIF-90@ GO/MDEA nanofluid: as a new class of multi-hybrid systems to enhance the performance of amine solutions in CO_2 absorption, J. Nat. Gas Sci. Eng. 74 (2020), 103110.
[46] L. Mohammadi, M.N. Zafar, M. Bashir, S.H. Sumrra, S.S. Shafqat, A.A. Zarei, H. Dahmardeh, I. Ahmad, M.I. Halawa, Modeling of phenol removal from water by NiFe2O4 nanocomposite using response surface methodology and artificial neural network techniques, J. Environ. Chem. Eng. 9 (2021), 105576.
[47] S. Ghanbari, B. Vaferi, Experimental and theoretical investigation of water removal from DMAZ liquid fuel by an adsorption process, Acta Astronaut. 112 (2015) 19–28.
[48] M. Karimi, B. Vaferi, S.H. Hosseini, M. Olazar, S. Rashidi, Smart computing approach for design and scale-up of conical spouted beds with open-sided draft tubes, Particuology 55 (2020) 179–190.
[49] B. Vaferi, R. Eslamloueyan, S. Ayatollahi, Application of recurrent networks to classification of oil reservoir models in well-testing analysis, Energy Sources Part A Recovery Util. Environ. Eff. 37 (2015) 174–180.
[50] Y. Tao, Y. Wang, M. Pan, S. Zhong, Y. Wu, R. Yang, Y. Han, J. Zhou, Combined ANFIS and numerical methods to simulate ultrasound-assisted extraction of phenolics from chokeberry cultivated in China and analysis of phenolic composition, Sep. Purif. Technol. 178 (2017) 178–188.
[51] J. Wang, P. Zhu, B. He, G. Deng, C. Zhang, X. Huang, An adaptive neural sliding mode control with ESO for uncertain nonlinear systems, Int. J. Control Autom. Syst. 19 (2021) 687–697.
[52] M. Shahriari-Kahkeshi, M. Moghri, Prediction of tensile modulus of PA-6 nanocomposites using adaptive neuro-fuzzy inference system learned by the shuffled frog leaping algorithm, E-Polymers 17 (2017) 187–198.
[53] M. Karimi, E. Aminzadehsarikhanbeglou, B. Vaferi, Robust intelligent topology for estimation of heat capacity of biochar pyrolysis residues, Measurement 183 (2021), 109857.
[54] W.C. Leong, R.O. Kelani, Z. Ahmad, Prediction of air pollution index (API) using support vector machine (SVM), J. Environ. Chem. Eng. 8 (2020), 103208.

[55] M. Nabavi, V. Nazarpour, A.H. Alibak, A. Bagherzadeh, S.M. Alizadeh, Smart tracking of the influence of alumina nanoparticles on the thermal coefficient of nanosuspensions: application of LS-SVM methodology, Appl. Nanosci. 11 (2021) 2113–2128.
[56] M.S.A. Sher Shah, W.-J. Kim, J. Park, D.K. Rhee, I.-H. Jang, N.-G. Park, J.Y. Lee, P. J. Yoo, Highly efficient and recyclable nanocomplexed photocatalysts of AgBr/N-doped and amine-functionalized reduced graphene oxide, ACS Appl. Mater. Interfaces 6 (2014) 20819–20827.
[57] A. Khalifeh, B. Vaferi, Intelligent assessment of effect of aggregation on thermal conductivity of nanofluids—comparison by experimental data and empirical correlations, Thermochim. Acta 681 (2019), 178377.
[58] M. Karimi, B. Vaferi, S.H. Hosseini, M. Rasteh, Designing an efficient artificial intelligent approach for estimation of hydrodynamic characteristics of tapered fluidized bed from its design and operating parameters, Ind. Eng. Chem. Res. 57 (2018) 259–267.
[59] B. Vaferi, M. Karimi, M. Azizi, H. Esmaeili, Comparison between the artificial neural network, SAFT and PRSV approach in obtaining the solubility of solid aromatic compounds in supercritical carbon dioxide, J. Supercrit. Fluids 77 (2013) 44–51.
[60] D.A. Wood, A. Choubineh, B. Vaferi, Transparent open-box learning network provides auditable predictions: pool boiling heat transfer coefficient for alumina-water-based nanofluids, J. Therm. Anal. Calorim. 136 (2019) 1395–1414.
[61] E. Davoudi, B. Vaferi, Applying artificial neural networks for systematic estimation of degree of fouling in heat exchangers, Chem. Eng. Res. Des. 130 (2018) 138–153.